frontiers in Materials

ORIGINAL RESEARCH
published: 13 September 2021
doi: 10.3389/fmats.2021.727925

Effect of the Alkalized Rice Straw Content on Strength Properties and Microstructure of Cemented Tailings Backfill

Shi Wang[1,2,3], *Xuepeng Song*[1,2,3]*, *Meiliang Wei*[1,2,3], *Wu Liu*[1,2,3], *Xiaojun Wang*[1,2,3]*, *Yuxian Ke*[1,2,3] *and Tiejun Tao*[4]

[1]School of Resources and Environmental Engineering, Jiangxi University of Science and Technology, Ganzhou, China, [2]Jiangxi Province Key Laboratory of Mining Engineering, Jiangxi University of Science and Technology, Ganzhou, China, [3]Engineering Research Center for High-efficiency Development and Application Technology of Tungsten Resources(Jiangxi University of Science and Technology), Ministry of Education, Ganzhou, China, [4]College of Civil Engineering, Guizhou University, Guiyang, China

OPEN ACCESS

Edited by:
Lijie Guo,
Beijing General Research Institute of Mining and Metallurgy, China

Reviewed by:
Erol Yilmaz,
Recep Tayyip Erdoğan University, Turkey
Shiqi Dong,
University of California, Los Angeles, United States

***Correspondence:**
Xuepeng Song
sxp9612@126.com
Xiaojun Wang
xiaojun7903@126.com

Specialty section:
This article was submitted to Structural Materials, a section of the journal Frontiers in Materials

Received: *20 June 2021*
Accepted: *02 August 2021*
Published: *13 September 2021*

Citation:
Wang S, Song X, Wei M, Liu W, Wang X, Ke Y and Tao T (2021) Effect of the Alkalized Rice Straw Content on Strength Properties and Microstructure of Cemented Tailings Backfill. Front. Mater. 8:727925. doi: 10.3389/fmats.2021.727925

The tailings and rice straw are waste by-products, and the storage of tailings on the ground and the burning of rice straws will seriously damage the ecological environment. In this study, the effect of different contents of alkalized rice straw (ARS; rice straw was alkalized with 4% NaOH solution) on the mechanical properties and microstructure of cemented tailings backfill (CTB; ARSCTB) was studied through uniaxial compressive strength (UCS), scanning electron microscopy (SEM), and X-ray diffraction (XRD) tests. The results indicated that 1) the UCS of ARSCTB could be improved by ARS. However, with the increase in the ARS content from 0.1 to 0.4 wt%, the UCS showed a monotonous decreasing trend. The UCS improvement effect was best when the ARS content was 0.1 wt%, and at 7, 14, and 28 days curing ages, the UCS increased rate was 6.0, 8.3, 14.7% respectively. 2) The tensile strength of ARSCTB was generally higher than that of CTB and positively correlated with the ARS content. The tensile strength increase rate was 24.1–34.2% at 28 days curing age. 3) The SEM test indicated that the ARS was wrapped by cement hydration products, which improves its connection with the ARSCTB matrix. ARS performed a bridging role, inhibited cracks propagation, and provided drag or pulling force for the block that is about to fall off. Therefore, the mechanical properties of ARSCTB were enhanced. However, under high ARS content, the inhibition of ARS on hydration reaction and the overlap between ARS were not conducive to the improvement of the UCS of ARSCTB. 4) The post-peak residual strength and integrity effect of ARSCTB were greater. It is recommended to add 0.1–0.2 wt% ARS to the backfill with high compressive strength requirements such as the empty field subsequent filling mining method and the artificial pillar. 0.3–0.4 wt% ARS is incorporated into backfill with high tensile strength requirements such as high-stage filling with lateral exposure and artificial roof. This study further makes up for the blank of the application of plant fiber in the field of mine filling and helps to improve the mechanical properties of backfill through low-cost materials.

Keywords: mechanical properties, alkalized rice straw, cemented tailings backfill, damage mode, microstructure evolution

INTRODUCTION

The mined-out areas formed during the mining of metal mines lead to the movement and fragmentation of rock layers, which in turn causes surface settlement in the mining area, unbalanced ecological environment, and even a series of problems such as safety accidents (Yang et al., 2017; Xu et al., 2019a; Huang et al., 2019; Zeng et al., 2020; Zheng et al., 2021). Meanwhile, a large number of tailings will inevitably be produced in the process of mineral processing. The tailings stored in the tailings pond not only occupy a lot of land resources but also causes pollution to groundwater and the surrounding ecological environment (Huynh et al., 2006; Yilmaz et al., 2015; Qi and Fourie, 2019; Hao et al., 2021). In addition, with the gradual depletion of shallow mineral resources, mines around the world have become deeper, high ground stress, and rockburst are the key factors leading to goaf instability (Hao et al., 2020). To solve the above problems, cemented tailings backfill (CTB) is widely used in underground mines around the world because of its ability to effectively control ground pressure, reduce surface settlement, and manage tailings (Liu et al., 2016; Wang et al., 2016; Zhao et al., 2017; Cao et al., 2019a; Yang et al., 2020). CTB is a complex composite material produced by mixing tailings (70–80 wt%), cementing materials (3–7 wt%), and a corresponding proportion of water, which is then transported to underground stopes by gravity or pumping (Yang et al., 2018; Xue et al., 2019a). The hardened filling body gradually has the ability to support the goaf, absorb, and transfer stress. However, in the process of filling mining, in addition to the quasi-static load of overlying strata, the backfill was also disturbed by the excavation blasting near the ore body, which was very easy to lead to the failure of the backfill. Therefore, the mechanical properties of the backfill are the key to its function. To improve the mechanical properties of the backfill, at present, domestic and foreign scholars used chemical reagents and/or synthetic fibers to enhance the mechanical properties of the backfill (Yi et al., 2015; Ma et al., 2016; Haruna and Fall, 2017; Chen et al., 2018; Manganea et al., 2018; Ouattara et al., 2018; Cao et al., 2019b; Xue et al., 2019b; Jiang et al., 2020; Kou et al., 2020; Cao et al., 2021; Cavusoglu et al., 2021; Koohestani et al., 2021), and certain research results have been achieved. However, the application of chemical reagents and synthetic fibers will increase the filling cost. Therefore, it is necessary to seek low-cost and wide-ranging admixtures to improve the mechanical behavior of the backfill.

In comparison with synthetic fibers, plant fibers have the advantages of low density, low cost, wide source (Xie et al., 2015; Xie et al., 2016; Wang et al., 2020). In terms of concrete, the application of plant fibers to improve the mechanical properties of concrete has always been a hot research topic (Chakraborty et al., 2013). Rahim et al. (2016) found that lime concrete added with rape straw and hemp exhibited good moisture absorption and buffer performance. Ammari et al. (2020) studied the physical and mechanical properties of concrete with barley straw and steel fiber, and the compressive strength of concrete was improved. Farooqi and Ali (2019) found that the compressive strength and flexural strength of concrete with wheat straw (wheat straw was soaked, boiled, and chemically treated) were all improved. Bederina et al. (2016) found that the flexural strength and shrinkage of concrete with barley straw treated with hot water, gasoline, varnish, and waste oil were enhanced. Zhang et al. (2020) concluded that the addition of rice straw significantly improved the tensile compression ratio and impact resistance of concrete. Xie et al. (2015) added different contents of rice straw to cement-based composites, which significantly improved the flexural strength and fracture toughness of cement-based composites. Chen et al. (2015) concluded that rice straw could control the development of cracks in the mortar, and the splitting toughness of the mortar was improved. Based on the above research, plant fiber can be used to improve the mechanical properties of cement-based materials, and as the oldest plant fiber used in cement-based materials, rice straw has been used for hundreds of years (Sun and Jiang, 2007; Xie et al., 2016; Zhang et al., 2020). Moreover, according to the statistics and calculation of FAOSTAT (the database of the United Nations Food and Agriculture Organization), in 2018, the amount of straw was nearly 800 million tons in China (Song et al., 2018; Li, 2020). Among them, the annual yield of rice straw reached 200 million tons. The phenomenon of random stacking and burning of rice straw is serious, and the utilization rate of resources is low [only a small percentage of rice straw is used as fodder and curtains or is biodegraded (Petrella et al., 2018; Wang et al., 2020)]. Most of the rice straw is burned in the field in spring and autumn, causing serious pollution to the surrounding environment and atmosphere (Chen et al., 2015; Ming et al., 2019). CTB is similar to cement-based materials, but there are some differences in aggregate source, size distribution of aggregate, and cement dosage between the two materials. Thus, it is of great significance to study the application of rice straw in the field of filling, to reduce the environmental pollution caused by rice straw burning, and to improve the utilization rate of resources and the mechanical properties of the backfill. Regarding the application of rice straw and other plant fibers in the field of filling, there are few related studies. Among them, Wang et al. (2020) studied the effect of alkalized rice straw of different lengths on the mechanical properties of CTB and found that the strength of CTB was significantly improved and was more sensitive to the rice straw length. As the length of the rice straw increased, the compressive strength of CTB increased first and then decreased. When the length of rice straw was 12 mm, the improvement effect of CTB strength was the best. However, the effect of different rice straw contents on the mechanical properties of CTB has not been studied. This would be resulted in an insufficient exploration of the application of plant fibers in the filling field. Therefore, it is necessary to carry out experimental research on the response of the mechanical properties of CTB with alkalize rice straw of different contents. It provides a more detailed theoretical and technical basis for the application of plant fiber in filling field.

Therefore, the aim of this experimental study is to provide a better understanding of the effect of different alkalized rice straw (ARS) contents on mechanical properties of CTB. To achieve this aim, a series of UCS and tensile strength tests were carried out. The strength changes, stress strain curve characteristics, and

TABLE 1 | Physical properties of the main tailings.

Property indexes	Porosity (vol%)	Specific gravity	Specific surface area (m^2/kg)	Content <20 μm (wt%)	Content <74 μm (wt%)	D_{10} (μm)	D_{50} (μm)	D_{90} (μm)	pH
Value	53.87	2.97	184.4	31.5	48.4	6.03	68.41	226.651	11

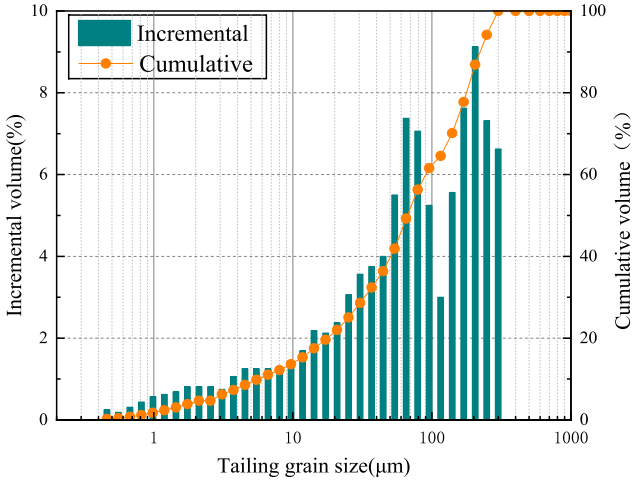

FIGURE 1 | Particle size distribution of unclassified tailings.

failure modes of CTB containing alkalized rice straw of different contents (ARSCTB) were determined. The influence mechanism of alkalized rice straw on CTB and ARSCTB strength was discussed by SEM and XRD tests.

MATERIALS AND METHODS

Experimental Materials and Characteristics

Tailings

The unclassified tailings were obtained from a copper mine in the Jiangxi Province, China. The particle size distribution of these tailings was analyzed using the Winner 2000 LPSA. The pycnometer method was used to measure the specific gravity, a small relative density meter was used to measure the unit density, and the pH value of the unclassified tailings slurry with an original mass concentration of 35% was measured on-site using the METTLER TOLEDO pH meter. The results are presented and depicted in **Table 1** and **Figure 1**, respectively. Particles in the tailings smaller than 74 μm account for about 48.4% of the total, which corresponds to a size classification of medium to fine. X-ray fluorescence analysis test (XRF-1800) was used to determine the main element content of the tailings, as shown in **Table 2**. The content of Si and Ca was relatively high, which was conducive to improve the strength of the backfill. The alkalinity of the tailings was M0 = 0.49, indicating that the tailings were acidic (<1).

Rice Straw

Rice straw was selected from the surrounding countryside of Ganzhou, Jiangxi Province. Rice straw is composed of cellulose, hemicellulose, lignin, and ash. Cellulose and hemicellulose are composed of polysaccharide units. Hydrolysis of polysaccharides under alkaline conditions will inhibit the hydration reaction of cement (Fan and Sheng., 2011; Xie et al., 2016; Wang et al., 2017). Some scholars used NaOH solution (4 wt%) to alkalized rice straw (ARS), which significantly reduced the inhibitory effect of rice straw on cement hydration reaction (Fan and Sheng, 2011; Chen et al., 2017; Wang et al., 2017; Liao et al., 2018). Thus, in this experiment, rice straw was soaked in NaOH solution (4 wt%) for 24 h, washed with water until the pH value was 7 ± 0.1, and then dried at 50°C. According to previous research (Wang et al., 2020), the length of fixing ARS is 12 mm, and the ARS content is 0, 0.1, 0.2, 0.3, 0.4 wt% of the cement quantity, respectively. The elastic modulus, bending deformation, and diameter of rice straw are 3.66 MPa, 3.17 mm, and 1.5–2.5 mm, respectively.

Binders and Water

The cementing material used in this test is ordinary Portland cement (P.O32.5) commonly used in mines. The specific surface area of the cement used is 2,105.2 cm^2/g, and the specific gravity is 2.97. Domestic water is used as the test water. The chemical composition of cement is shown in **Table 3**.

EXPERIMENTAL METHOD

The test procedure is shown in **Figure 2**. The brief introduction to the test steps is as follows:

Sample Preparation

The mix proportion for the CTB and ARSCTB mixtures used a cement-to-tailings (c / t) ratio (dry weight) of 1:4 and a solid content of 74 wt%. ARS was added to filling materials at 0, 0.1, 0.2,

TABLE 2 | Composition of the main elements of the unclassified tailings (%).

Composition/%	SiO_2	CaO	MgO	Al_2O_3	Fe_2O_3	SO_2	PbO_2	MnO_2	K_2O	P_2O_5	CuO
Content	33.02	15.68	1.82	2.56	10.37	4.55	0.0095	0.085	0.37	0.049	0.065

TABLE 3 | The chemical composition of cement.

Compositions	CaO	SiO_2	Al_2O_3	Fe_2O_3	MgO	SO_2	Na_2O	Other
wt%	63.66	21.26	4.5	2.8	1.66	2.58	0.18	3.36

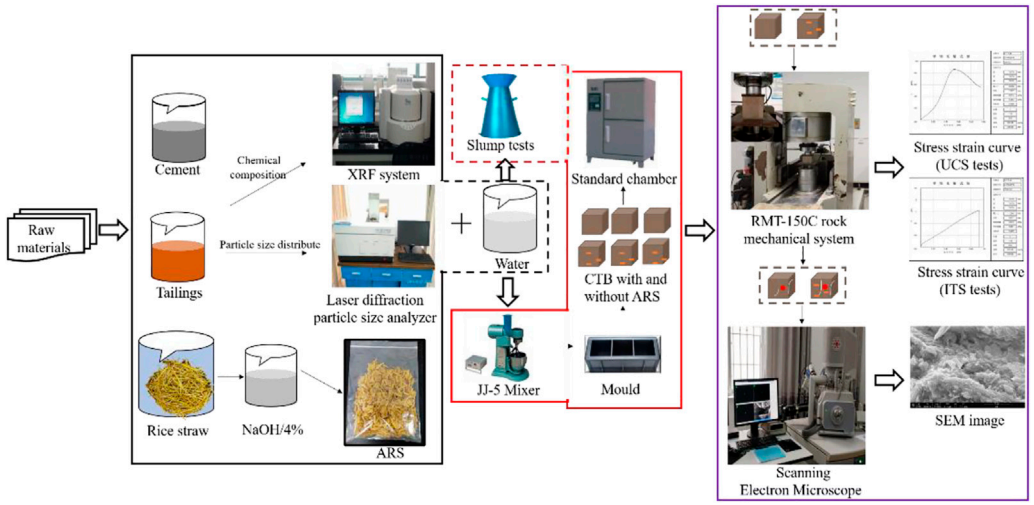

FIGURE 2 | The experimental flowchart.

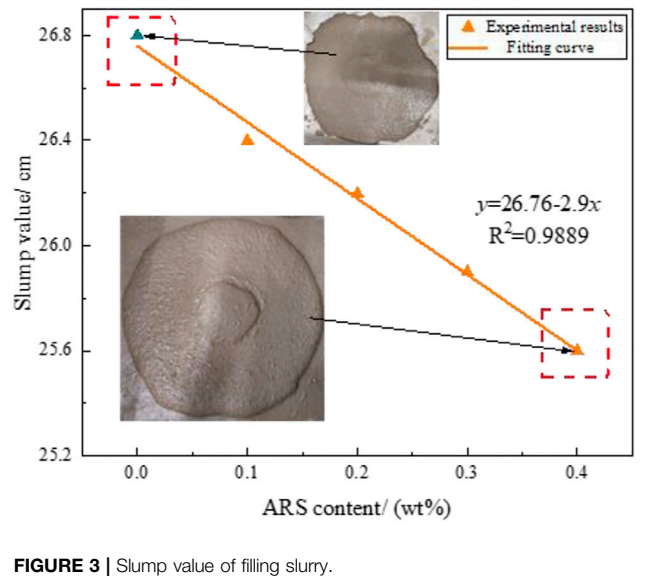

FIGURE 3 | Slump value of filling slurry.

0.3, and 0.4 wt% of the cement mass. When preparing the sample, cement and tailings were first mixed evenly, and then ARS was added and mixed again. Finally, a proper amount of water was added and stirred by a JJ-5 mixer for 5 min to ensure even mixing. Part of CTB and ARSCTB slurries were tested for slump (rice straw had strong water absorption capacity, and with increased ARS content, the fluidity of filling slurry would inevitably be affected. Hence, according to Standard Test Method for Slump of Portland Cement Concrete (ASTM C143/C143M-2015), slump test of filled slurry with ARS was carried out using cone slump cone (upper diameter: 10 cm, lower diameter: 20 cm, height: 30 cm) (Wang and Chen, 2016; Zheng et al., 2016; Deng, 2017; Chen et al., 2020). The results were shown in **Figure 3** and **Table 4**. With the ARS content increase from 0 to 0.4 wt%, the slump value decreased from 26.8 to 25.6 cm, showed a linearly decreasing trend. They have a high linear function relationship (R^2 = 0.9889, where x and y represent the ARS content and slump value, respectively). The results show that ARS can affect the fluidity of the filling slurry, which is due to its high water absorption capacity, which reduces the free water content in the fresh filling slurry, resulting in the decrease of the fluidity of

TABLE 4 | The experiment scheme design of uniaxial compressive strength tests and tension tests.

NO.	c/ta	W/ (wt%)b	L (%)/ (mm)c	C/ (wt%)d	Slump/ (cm)
C-0			0	0	26.8
C-1			12	0.1	26.4
C-2	1:4	74	12	0.2	26.2
C-3			12	0.3	25.9
C-4			12	0.4	25.6

[a]*dry mass ratio of cement to tailings.*
[b]*mass concentration.*
[c]*ARS length.*
[d]*ARS content.*

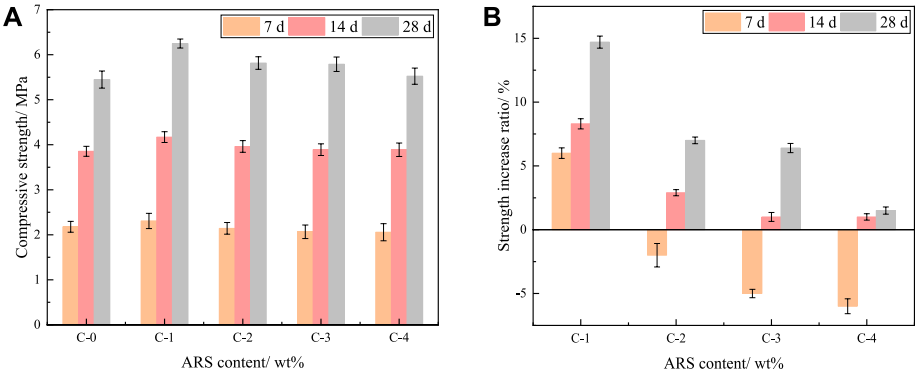

FIGURE 4 | The UCS of CTB and ARSCTB.

the fresh filling slurry (Sathiparan and De Zoysa, 2018; Chen et al., 2020). Meanwhile, since the maximum ARS content in this test was only 0.4 wt% of the cement quantity, it had little effect on the slump of the filling slurry (the maximum reduction rate was only 4.8%). The addition of ARS could ensure that the filling slurry had good fluidity. The remaining part of the filling slurry was poured into a cube mold (70.7 mm), and after demolding, the samples were placed in an HBY-40B standard curing box (20°C ± 1°C, 90 ± 5%). The experimental design is presented in **Table 4**.

Uniaxial Compressive Strength and Tensile Strength Tests

After the desired curing time (7, 14, and 28 days), the UCS test was conducted on CTB and ARSCTB (CTB and ARSCTB were cube samples with a size of 70.7 mm. The upper and lower end faces of the samples were polished before testing) according to the standard ASTMC39/C39M-18. The RMT-150C rock mechanics test system was used. The backfill was loaded continuously at a constant speed of 0.6 mm/min, the maximum load was 1,000 kN, and the piston stroke was 50 mm, recorded once every 0.5 s. On this basis, the tensile strength was tested at the same loading rate. The mechanical parameters and stress strain curves of the backfill were obtained. Three samples were tested for each backfill formulation, and the average values of the UCS and tensile strength were calculated.

Scanning Electron Microscopy and X-Ray Diffraction Tests

Microstructural tests of CTB and ARSCTB were performed by SEM equipment (XL30W/TMP, United States) at 28 days curing time. The samples were crushed and cored, and the cement hydration reaction was terminated with anhydrous ethanol after 28 days (Wang et al., 2020). The samples were sprayed with gold to improve conductivity. The samples were placed into the SEM sample chamber, a vacuum was created, and the interaction between ARS and the ARSCTB matrix was observed. In addition, XRD (Smart apex II, United States) was used to determine the type and intensity of hydration products of CTB and ARSCTB. In this experiment, the scanning speed was 10 deg/min, and the range of 2 θ was 10–90°.

RESULTS AND DISCUSSION

The Effect of Rice Straw was Alkalized With 4% NaOH Solution Content on the Uniaxial Compressive Strength of CTB and ARSCTB

Figure 4 shows the UCS test results of CTB and ARSCTB at 7, 14, and 28 days curing ages. As the figure shows: 1) at 14 days curing age, the UCS of CTB was 3.85 MPa, and the UCS of ARSCTB decreased gradually from 4.17 MPa with 0.1 wt% ARS to 3.89 MPa with 0.4 wt%, that is, the increased rate of the UCS of ARSCTB decreased from 8.3 to 1.0%. 2) When the ARS content was 0.1 wt%, at 7, 14, and 28 days curing age, compared with CTB, the UCS of ARSCTB increased by 6.0, 8.3, 14.7%, respectively. When the ARS content was 0.2, 0.3, 0.4 wt%, it had the same properties, that is, with the increased curing age, the better the improvement effect of ARS on the UCS of ARSCTB; 3) At 7 days curing age, when the ARS content was 0.2, 0.3, 0.4 wt%, the UCS of ARSCTB was reduced by 2.0, 5.0, 6.0% compared with CTB, and the UCS of other ARSCTBs was higher than the corresponding CTB.

The above three conclusions are mainly attributed to the following three reasons. 1) ARS plays a bridging role in the ARSCTB matrix. **Figure 5** is a schematic diagram of the distribution of ARS in the ARSCTB matrix. As shown in **Figure 5**, ARS has a high adhesive strength with the ARSCTB matrix, which can inhibit the crack propagation and exert a drag force on the block that is about to fall off; thus, the effective stress area of ARSCTB is increased, and the strength is improved (Wang et al., 2020; Ramli et al., 2013; Bederina et al., 2016) (conclusion 1) and 2) ARS inhibits cement hydration reaction. Although the rice straw is alkalized, there is a slight inhibition of cement hydration (Wang et al., 2017). With the increase of ARS content, the inhibition effect of ARS on cement hydration reaction gradually appears, which leads to the decrease of adhesive strength between ARS and the ARSCTB matrix, which weakens the bridging effect and crack inhibition effect, and the UCS of ARSCTB decreases. This phenomenon is also supported by XRD results, as shown in **Figure 6**. From **Figure 6A**, the main hydration products of CTB and ARSCTB

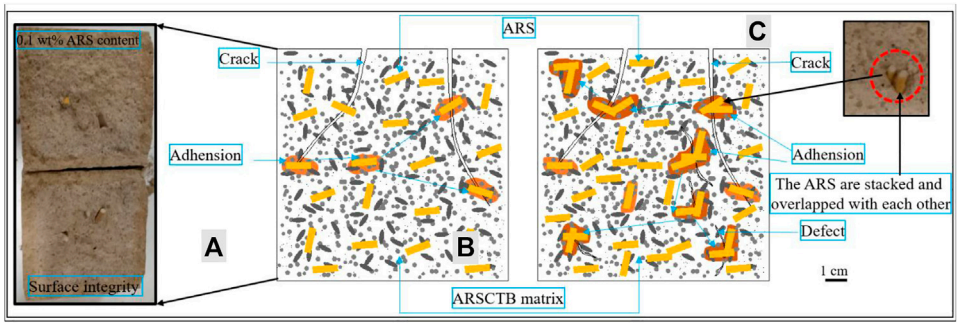

FIGURE 5 | Two-dimensional distribution diagram of ARS (**A**: 0.1 wt%; **B**: 0.4 wt%).

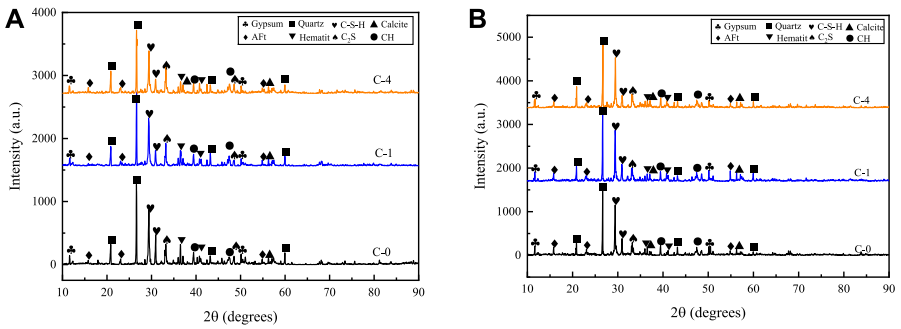

FIGURE 6 | X-ray diffraction (XRD) patterns of CTB and ARSCTB (**A**-7 days; **B**-28 days).

are calcium silicate hydrate (C-S-H), calcium hydroxide (CH), and ettringite (AFt) at 7 days curing age. When the content of ARS is 0.1 wt%, compared with CTB, the change of diffraction peak of hydration products is small. It indicated that the ARS content is less, and the inhibition effect of ARS on cement hydration is not obvious. Therefore, the adhesive force between ARS and the ARSCTB matrix is high, and the bridging effect is dominant, which effectively improved the internal structure of ARSCTB. When the ARS content is 0.4 wt%, the diffraction peak of hydration products decreases obviously. It indicated that the inhibition effect of ARS on cement hydration reaction is enhanced, which leads to the decrease of adhesive strength between ARS and the ARSCTB matrix, so the UCS of ARSCTB decreases. As the curing age increases, cement hydration products increase (Xu et al., 2019b), which can also be found in **Figure 6B** (the diffraction peak intensity of hydration products increases), and it can be seen from **Figure 6B** that the diffraction peak intensities of hydration products of CTB and ARSCTB have no obvious difference. It indicated that with the increase in curing age, the inhibition effect of ARS on cement hydration reaction is weakened. Thus, the degree of the connection between ARS and the ARSCTB matrix is enhanced, and the adhesive force and friction between ARS and the ARSCTB matrix increase significantly. Therefore, the UCS of ARSCTB is higher than that of CTB, and the bridging effect of ARS is dominant at 14 and 28 days curing ages regardless of the ARS content (conclusion 2 and 3). 3) ARS was randomly dispersed in the ARSCTB matrix (**Figure 5A**). With increased ARS content, ARS overlapped each other in the ARSCTB matrix (Xu et al., 2019a), which caused the decrease of adhesive strength between ARS and the ARSCTB matrix, and defects were generated (as shown in **Figures 5B,C**), which was another reason why the UCS of ARS decreased gradually with increased ARS content (conclusion 1)). In summary, the addition of an appropriate amount of ARS can improve the compressive strength of the backfill, which is consistent with the previous results (Chen et al., 2020). However, compared with the previous research results (Chen et al., 2020), the improvement effect of ARS on the compressive strength of backfill in this study is relatively low, which may be related to the preparation of rice straw (rice straw is alkalized in this study, and the shape of rice straw is circular tube, while the rice straw used by Chen et al. (2017) is flocculent).

The Effect of Rice Straw was Alkalized With 4% NaOH Solution Content on the Tensile Strength of CTB and ARSCTB

Figure 7 shows the tensile strength test results of CTB and ARSCTB at 7, 14, and 28 days curing ages. As shown in **Figure 7**, the tensile strength of CTB was 0.27 MPa at 7 days curing age. As the ARS content gradually increased from 0.1 to

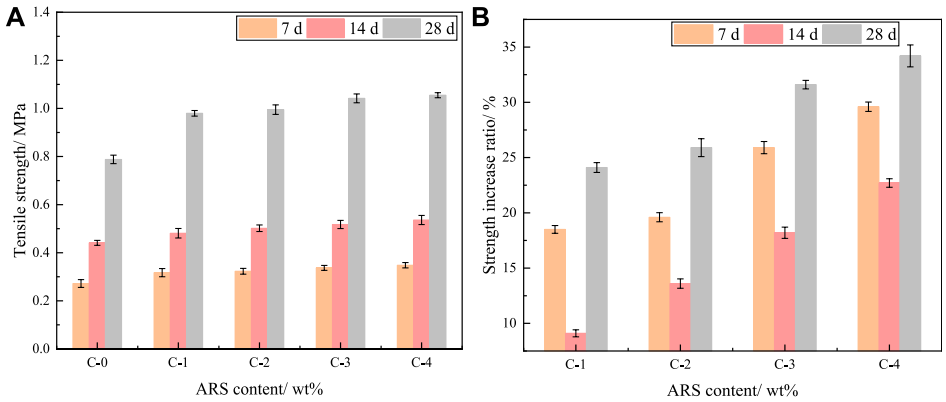

FIGURE 7 | The tensile strength of CTB and ARSCTB.

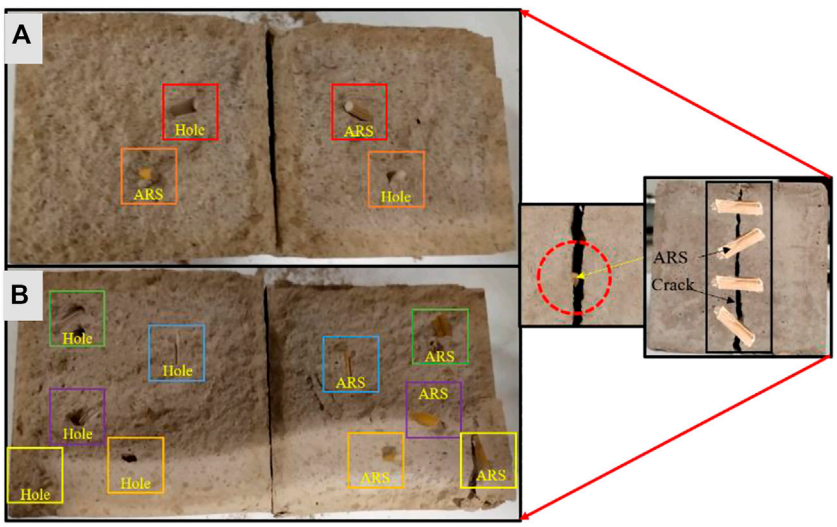

FIGURE 8 | The split surface of ARSCTB (a: 0.1 wt%, 0.4 wt%).

0.4 wt%, the tensile strength of ARSCTB increased from 0.32 to 0.36 MPa, and the increased rate of tensile strength was 18.5–29.6%. Meanwhile, the changing trend of tensile strength was the same at 14, 28 days curing ages. The increased rate of tensile strength was 9.1–22.7% and 24.1–34.2%; that is, the tensile strength of ARSCTB was generally higher than CTB. The tensile strength was positively correlated with the ARS content. This conclusion is mainly attributed to the following two reasons. 1) ARS plays as a bridging role in the ARSCTB matrix. As mentioned earlier, ARS is randomly distributed inside the ARSCTB matrix. when the ARCTB tensile failure occurs, ARS may have penetrated the positions where ARSCTB is damaged by tension, similar to "grouting anchor" (bridging effect), as shown in **Figure 8**. The adhesive force between ARS and the ARSCTB matrix can inhibit the crack propagation (Xue et al., 2019a; Wang et al., 2020) and provide pulling force for the blocks on both sides of the crack. Therefore, the tensile stress was transferred from the ARSCTB matrix to ARS, and the pulling out of the ARS from the matrix consumed energy, thereby the tensile strength of ARSCTB is enhanced. 2) With the increase of ARS content, the number of ARS on both sides of tensile crack is increased. **Figures 8A,B** show the split surface of tensile strength test of ARSCTB with ARS content of 0.1 and 0.4 wt%, respectively. It can be seen from the figure that with the increase of ARS content, the number of ARS at the split surface increases obviously (for instance, the number of ARS increased from two at 0.1% to five at 0.4%, and there was a positive correlation between them). The bridging effect of ARS is strengthened, and the inhibition effect of ARS on cracks is enhanced. Thus, the pulling force provided by ARS for both sides of the crack is increased, and more ARSs consume more capacity when pulling out of the ARSCTB matrix, contributing to the improvement of the tensile strength of ARSCTB. In addition, the strengthening bridging effect of ARS can also make up for the inhibition of ARS on cement hydration

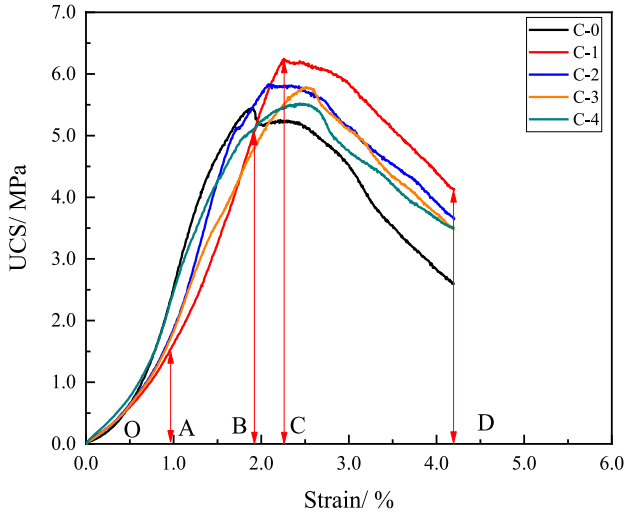

FIGURE 9 | Stress-strain curves of the UCS of CTB and ARSCTB.

at 7 days curing age, which can also be clearly found in the changing trend of the ARSCTB tensile strength.

Analysis of the Stress Strain Curves of CTB and ARSCTB

The Stress Strain Curves of Uniaxial Compressive Strength

Figure 9 shows the stress strain curves of the UCS test of CTB and ARSCTB at 28 days curing age. The failure process of CTB and ARSCTB is divided into four stages: 1) pore compaction stage (OA); 2) linear elasticity stage (AB); 3) plastic yield stage (BC); 4) failure stage (CD) (Cao et al., 2019a; Xue et al., 2019b; Wang et al., 2020). The detailed description of each stage of the curve is as follows:

In the OA stage, the curves were concave upward. Under the initial loading condition, the internal pores were compressed and closed or broken under the action of external force (28 days curing age, the backfill had high brittleness). In this stage, the strain of ARSCTB was greater than CTB. This may be due to the existence of ARS which is not completely filled by the cement tailings, resulting in increased pores. Thus, strain was increased. This phenomenon was consistent with the results of previous studies (Wang et al., 2020). In AB stage, the backfill entered the elastic deformation stage, and the curves of all samples are approximately straight line. The slope of the ARSCTB curve was smaller than CTB, and the time to break the threshold was longer. In BC stage, the cracks in the backfill gradually expanded, and the curves were convex, and gradually reached the peak strength (Cheng et al., 2018). At this stage, the peak strength of ARSCTB was generally higher than that of CTB. At this stage, ARS was the main action stage (Wang et al., 2020; Xue et al., 2020), which played a bridging role in the ARSCTB matrix. The further propagation and convergence of cracks were restrained, the stress concentration at the crack tip was relieved, and the drag force was generated on the block of ARSCTB, so that the compressive stress was evenly distributed on the top and bottom of ARSCTB, and the strength of ARSCTB was improved. In the CD stage, after the peak strength, the crack evolution was intensified, and the load continues to be applied, and the compressive strength rapidly decreases and gradually flattens. It can be found that all the samples had a certain residual strength, the residual strength of ARSCTB was significantly higher than that of CTB, and the residual strength decreased with the increase of ARS content. This is because ARS played a bridging role in the ARSCTB matrix and produced a drag force on the block. As a result, the abscission of block of ARSCTB was reduced, and the stress area of ARSCTB was increased. The residual strength of ARSCTB was improved, and the bearing capacity was more after failure. However, the increase in ARS content increased the probability of ARS overlapping and cross, and then reduced the post-peak bearing capacity. The UCS and post-peak residual strength of the backfill are improved by the addition of ARS. It follows that in actual filling operations, ARSCTB can better ensure the stability of the goaf and improve the safety of downhole operations.

The Stress Strain Curves of Tensile Strength

Figure 10 shows the stress strain curve of tensile strength tests for CTB and ARSCTB at 28 days curing age. As shown in **Figure 10**, from the overall view, a higher brittleness was exhibited by CTB and ARSCTB, when the tensile stress reached the extreme tensile strength value, the stress was reduced to zero instantly. However, the peak tensile strength of ARSCTB was higher at 28 days curing age (corresponding to the results of tensile strength test), and the peak strain of ARSCTB was greater. The bridging effect of ARS in the ARSCTB matrix exerted a pilling force on the blocks of both sides of the crack, which improved the tensile strength of ARSCTB, inhibited the crack propagation, and slowed down the failure of ARSCTB. Moreover, the increase of peak strain can delay damage under tensile stress, which is beneficial to the

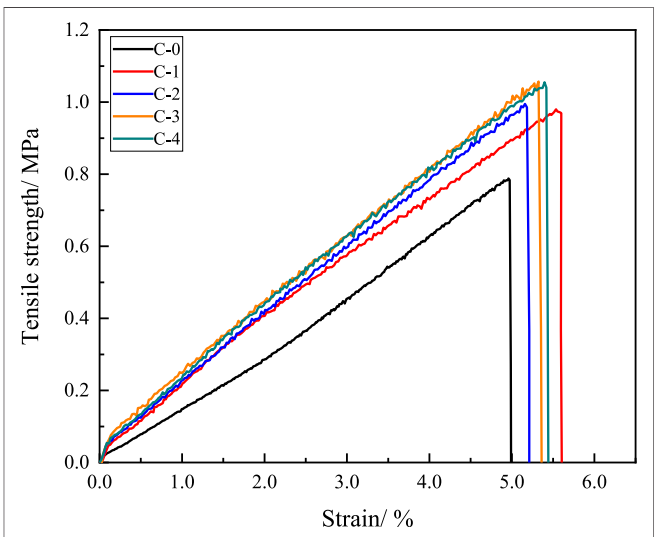

FIGURE 10 | Stress-strain curves of the tensile strength of the CTB and ARSCTB.

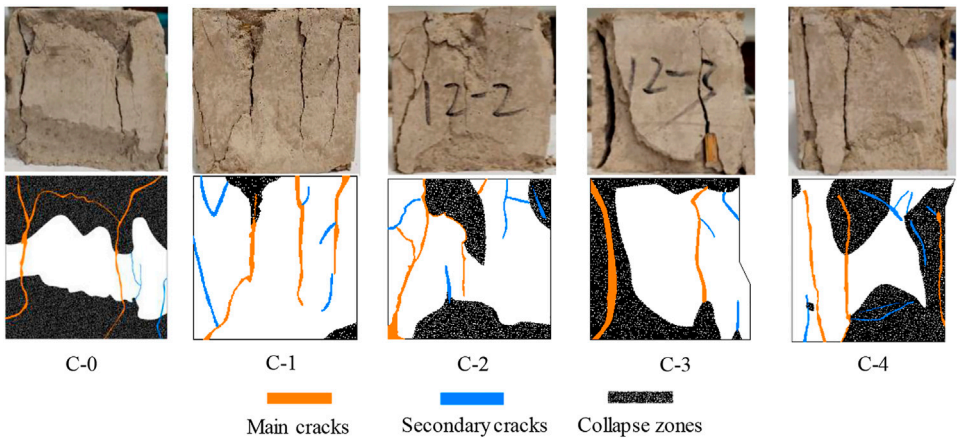

FIGURE 11 | Failure mode of CTB and ARSCTB.

safety of downhole operation. Meanwhile, ore dilution and high brittleness of the backfill can be reduced.

Analysis of Damage Mode of CTB and ARSCTB

Figure 11 shows the failure modes of CTB and ARSCTB at 28 days curing age. It can be seen from **Figure 11** that there are differences in failure mode and damage degree between CTB and ARSCTB, indicating that the internal structure of ARSCTB is changed by ARS. As shown in **Figure 11C–0**, the failure mode of CTB was mainly tensile failure; accompanied by shear failure, two nearly parallel main cracks penetrated the upper and lower sides of CTB, and they were connected by a third main crack, resulting in the block was about to separate from the CTB matrix. Two collapse areas were generated during the compression process (the area of the collapsed area was larger). CTB was seriously damaged under uniaxial compression, and the bearing capacity was poor after damage, which corresponded to the lower post-peak residual strength in **Figure 9**. However, the failure mode of ARSCTB was more complex. The failure mode of ARSCTB was tension shear mixed failure, which may be related to the significant increase of tensile strength of ARSCTB in **Figure 5**. It can be found from **Figures 11C1–4** that the main crack of ARSCTB was narrow and did not penetrate the upper and lower parts of ARSCTB, and there was no obvious large body falling off. Meanwhile, ARSCTB had more secondary cracks, and the secondary cracks were not connected with each other under this strain condition, which had little effect on the strength. In addition, with increased ARS content, the area of the ARSCTB collapse zone increased gradually. This was because the increased rate of ARS content caused the overlap of ARS in the ARSCTB matrix, which reduced the adhesive force between ARS and the ARSCTB matrix, resulting in the increased collapse area. This phenomenon was consistent with the conclusion in **Figure 4**. From overall view, after the UCS test, the integrity of ARSCTB was higher, and the block did not fall off. This phenomenon corresponded to the higher residual strength of the ARSCTB stress strain curve. In addition, when the ARS content was 0.1 wt%, ARSCTB was most integrated after UCS test, which was consistent with the changing trend of UCS in **Figure 4**. The integrity of ARSCTB is improved by ARS, and then the stability of backfill is enhanced, which is beneficial for backfill to effectively support goaf, maintain its own self-supporting ability, better play its different functions, and improve safety of downhole operation. Meanwhile, the ARS content can be adjusted by the actual filling mining method, and then the different mechanical behaviors of the backfill can be obtained, as described in the following the engineering suggestions.

Analysis of Microstructure Evolution of CTB and ARSCTB

The mechanical properties of ARSCTB were significantly improved by the addition of ARS. To understand the micro-scale interaction relationship between ARS and the ARSCTB matrix, and based on the influence of ARS content on the UCS and tensile strength of ARSCTB, the SEM test was carried out on the representative backfill samples (C-0, C-1, C-4) at 28 days curing age, as shown in **Figure 12**. It can be seen from **Figures 12C–0,1,4** that the microstructure of CTB and ARSCTB had no obvious difference at 28 days curing age, with dense structure and less pores, and the inhibition effect of ARS on cement hydration was negligible (it is consistent with the XRD results in **Figure 6B**). Therefore, the change of the internal structure of the ARSCTB matrix by ARS is the main reason for its strength improvement. **Figures 12C–1i,4i** show the microscopic interaction relationship between ARS and the ARSCTB matrix when the ARS content was 0.1 and 0.4 wt%, respectively. It can be seen from the figure that the end and surface of ARS were wrapped by cement hydration products, and the adhesive strength between ARS and the ARSCTB matrix was improved, which help ARS play a bridging role in the ARSCTB matrix, and the crack propagation was restrained, providing a drag force or pulling force for the block that is about to fall off (Chen et al., 2020; Wang et al., 2020). Thus, the mechanical properties of ARSCTB were improved, the post-peak residual strength was increased, and the

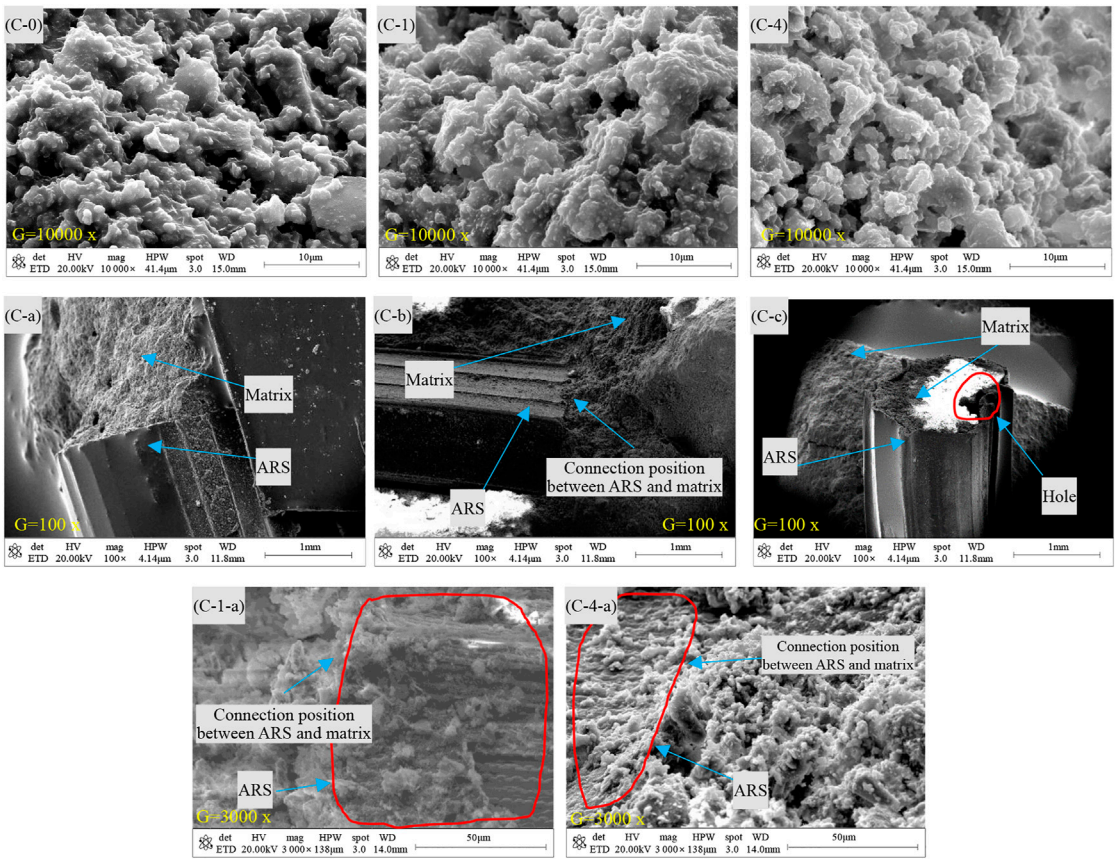

FIGURE 12 | SEM images of CTB and ARSCTB (G is the magnification).

integrity of ARSCTB was enhanced (consistent with the results in **Figure 4** and **Figure 11**). In addition, the rough texture of the ARS surface increased its friction with the ARSCTB matrix and further improved the adhesive strength between ARS and the ARSCTB matrix (strengthening the bridging effect of ARS). **Figures 12C–i,ii,iii** show the microscopic interaction between ARS (ARS content is 0.4 wt%) and the ARSCTB matrix. It can be seen from the figure that ARS was filled with cement tailings and connected to the ARSCTB matrix as a whole without obvious cracks (**Figures 12C–i,ii**), which hold ARS play a better bridging role, the morphology of ARS in the backfill matrix was consistent with that of Chen et al., 2020. In addition, in **Figure 12–Ciii**, there were holes in ARS that were not filled with cement tailings, but ARS was not damaged under external force, which corresponded to the large strain at the initial stage of the stress strain curve of ARSCTB in **Figure 9**.

ENGINEERING SUGGESTIONS

The mechanical properties of the backfill in filling mining method are the key to control ground pressure, reduce surface subsidence, and provide safe working environment for workers. Therefore, the backfill must have enough stability. Based on this study, the UCS and tensile strength of ARSCTB were higher than those of CTB at 28 days curing age regardless of the ARS content (especially at 0.1 wt% ARS, the UCS of ARSCTB was best improved, and when this content of ARS was added to the backfill, the strength of ARSCTB was significantly improved compared with the strength of the backfill required by the mine, which ensured the safety of underground operation). However, the UCS and tensile strength of ARSCTB have negative correlation and positive correlation with the ARS content. Therefore, for the application of ARS in actual filling, the following suggestions are presented: 1) In the open stope and subsequent filling method with pillars, the compressive strength of the backfill is the key to its stability. Therefore, it is recommended to add 0.1 wt% ARS to the backfill. 2) In the high-stage subsequent filling mining method with two-step stoping, the backfill is exposed laterally during the second step mining, and the backfill is prone to tensile failure under the action of ground pressure and blasting stress wave. It is recommended to add 0.3–0.4 wt% ARS. 3) In the downward slicing or drift filling mining method, as artificial false roof, the backfill is prone to tensile failure, which increases the mining risk. Therefore, it is recommended to add 0.4 wt% ARS. 4) When the backfill is used as artificial pillar for residual pillar mining, the compressive strength of the backfill is required to be high. Therefore, it is recommended to add 0.1 wt% ARS.

CONCLUSIONS

1) The UCS of ARSCTB can be improved by ARS, and it is positively correlated with curing age. However, with the ARS content increases from 0.1 to 0.4 wt%, the UCS of ARSCTB gradually decreases. When the ARS content is 0.1 wt%, the UCS improvement effect is best, and the UCS increased rate is 6.0, 8.3, 14.7% at 7, 14, and 28 days curing age.

2) With the ARS content increases from 0.1 to 0.4 wt%, the increased rates of tensile strength of ARSCTB at 7, 14, and 28 days are 18.5–29.6%, 9.1–22.7%, and 24.1–34.2%, respectively. The tensile strength of ARSCTB is generally higher than that of CTB and is positively correlated with the ARS content.

3) The failure mode of ARSCTB is complex, mainly tensile shear mixed failure. However, ARSCTB has higher integrity after failure. ARSCTB is most integrated after the UCS test, when the ARS content was 0.1 wt%. Meanwhile, ARSCTB has higher residual strength and greater bearing capacity after failure.

4) The microstructure shows that ARS is wrapped by the cement hydration products and has a high adhesive force with the ARSCTB matrix. ARS plays a bridging role in the matrix. The crack propagation is restrained. However, after a content of about 0.2–0.3 wt%, the inhibition of ARS on hydration reaction and the overlap between ARS are not conducive to the improvement of the UCS of ARSCTB.

5) In the actual filling operation, it is recommended to add 0.1 wt% of ARS to the backfill of open stope and subsequent filling method, and 0.3–0.4 wt% of ARS to the backfill that needs to be laterally exposed in the high stage, 0.4 wt% ARS is added to the backfill of the false roof, and 0.2–0.3 wt% ARS is added to the backfill used as the artificial pillar mining residual pillar.

The change of ARS content significantly affects the strength of changing trend of backfill, which indicates that it is valuable to study the effect of ARS content on the mechanical properties of backfill. Meanwhile, according to the influence of ARS content on UCS and tensile strength, ARS contents can be determined according to the actual filling situation. Moreover, it is a green and sustainable development method to improve the mechanical properties of backfill by using rice straw waste with low cost and wide sources.

DATA AVAILABILITY STATEMENT

The original contributions presented in the study are included in the article/Supplementary Material; further inquiries can be directed to the corresponding authors.

ETHICS STATEMENT

Written informed consent was obtained from the individual(s), and minor(s)' legal guardian/next of kin, for the publication of any potentially identifiable images or data included in this article.

AUTHOR CONTRIBUTIONS

All authors listed have made a substantial, direct and intellectual contribution to the work, and approved it for publication.

FUNDING

This study was supported by the National Natural Science Foundation of China (No. 51804134, No. 51804135), the Natural Science Foundation of Jiangxi Province (No. 20181BAB216013), and the Program of Qingjiang Excellent Young Talents, Jiangxi University of Science and Technology (JXUSTQJYX2019007).

REFERENCES

Ammari, M. S., Belhadj, B., Bederina, M., Ferhat, A., and Quéneudec, M. (2020). Contribution of Hybrid Fibers on the Improvement of Sand concrete Properties: Barley Straws Treated with Hot Water and Steel Fibers. *Constr. Build. Mater.* 233, 117374. doi:10.1016/j.conbuildmat.2019.117374

Bederina, M., Belhadj, B., Ammari, M. S., Gouilleux, A., Makhloufi, Z., Montrelay, N., et al. (2016). Improvement of the Properties of a Sand concrete Containing Barley Straws - Treatment of the Barley Straws. *Constr. Build. Mater.* 115, 464–477. doi:10.1016/j.conbuildmat.2016.04.065

Cao, S., Yilmaz, E., and Song, W. (2019a). Fiber Type Effect on Strength, Toughness and Microstructure of Early Age Cemented Tailings Backfill. *Constr. Build. Mater.* 223, 44–54. doi:10.1016/j.conbuildmat.2019.06.221

Cao, S., Yilmaz, E., Song, W., Yilmaz, E., and Xue, G. (2019b). Loading Rate Effect on Uniaxial Compressive Strength Behavior and Acoustic Emission Properties of Cemented Tailings Backfill. *Constr. Build. Mater.* 213, 313–324. doi:10.1016/j.conbuildmat.2019.04.082

Cao, S., Xue, G., Yilmaz, E., and Yin, Z. (2021). Assessment of Rheological and Sedimentation Characteristics of Fresh Cemented Tailings Backfill Slurry. *Int. J. Mining, Reclam. Environ.* 35 (5), 319–335. doi:10.1080/17480930.2020.1826092

Cavusoglu, I., Yilmaz, E., and Yilmaz, A. O. (2021). Sodium Silicate Effect on Setting Properties, Strength Behavior and Microstructure of Cemented Coal Fly Ash Backfill. *Powder Technol.* 384, 17–28. doi:10.1016/j.powtec.2021.02.013

Chakraborty, S., Kundu, S. P., Roy, A., Adhikari, B., and Majumder, S. B. (2013). Polymer Modified Jute Fibre as Reinforcing Agent Controlling the Physical and Mechanical Characteristics of Cement Mortar. *Constr. Build. Mater.* 49, 214–222. doi:10.1016/j.conbuildmat.2013.08.025

Chen, H. T., Ming, X. L., Liu, S., Zhang, Y., and Zhang, H. C. (2015). Optimization of Technical Parameters for Making Mulch from Waste Cotton and Rice Straw Fiber. *Trans. Chin. Soc. Agric. Eng.* 20, 300–308. doi:10.11975/j.issn.1002-6819.2015.13.041

Chen, B., Lu, Y. B., Su, S., and Luo, D. (2017). Influence of Straw Fiber on Tensile Properties of Concrete. *China Concr. Cem. Prod.* (10), 85–88. doi:10.19761/j.1000-4637.2017.10.020

Chen, X., Shi, X., Zhou, J., Chen, Q., Li, E., and Du, X. (2018). Compressive Behavior and Microstructural Properties of Tailings Polypropylene Fibre-Reinforced Cemented Paste Backfill. *Constr. Build. Mater.* 190, 211–221. doi:10.1016/j.conbuildmat.2018.09.092

Chen, X., Shi, X., Zhou, J., Yu, Z., and Huang, P. (2020). Determination of Mechanical, Flowability, and Microstructural Properties of Cemented Tailings Backfill Containing rice Straw. *Constr. Build. Mater.* 246, 118520. doi:10.1016/j.conbuildmat.2020.118520

Cheng, A., Zhang, Y., Dai, S., Dong, F., Zeng, W., and Li, D. (2018). Spatiotemporal Evolution Law and Fracture Prediction of Acoustic Emission Parameters of Uniaxial Compressed Cemented Backfill. *Rock Soil Mech.* 40, 2–9. doi:10.16285/j.rsm.2018.1940

Deng, X. J. (2017). Ground Control Mechanism of Mining Extra-thick Coal Seam Using Upward Slicing Longwall-Roadway Cemented Backfilling

Technology. Xuzhou, China: China University of mining and technology. Doctoral Dissertation.

Fan, H., and Sheng, L. (2011). Experimental Studies on Performance of Cement-Based Straw Fiber Material. *J. Anhui Agric. Univ.* 38, 159–162. doi:10.13610/j.cnki.1672-352x.2011.04.015

Farooqi, M. U., and Ali, M. (2019). Effect of Pre-treatment and Content of Wheat Straw on Energy Absorption Capability of concrete. *Construct. Build. Mater.* 224, 572–583. doi:10.1016/j.conbuildmat.2019.07.086

Hao, X., Du, W., Zhao, Y., Sun, Z., Zhang, Q., Wang, S., et al. (2020). Dynamic Tensile Behaviour and Crack Propagation of Coal under Coupled Static-Dynamic Loading. *Int. J. Mining Sci. Technol.* 30 (5), 659–668. doi:10.1016/j.ijmst.2020.06.007

Hao, X., Zhang, Q., Sun, Z., Wang, S., Yang, K., Ren, B., et al. (2021). Effects of the Major Principal Stress Direction Respect to the Long axis of a Tunnel on the Tunnel Stability: Physical Model Tests and Numerical Simulation. *Tunnelling Underground Space Technol.* 114 (7), 103993. doi:10.1016/j.tust.2021.103993

Haruna, S., and Fall, M. (2017). "Enhanced Flow Ability and Mechanical Characteristics of Cemented Paste Backfill with a Chemical Admixture," in Proceedings of the 12th International Symposium on Mining with Backfill (Ottawa, Canada: Minefill).

Huang, Y., Li, J., Ma, D., Gao, H., Guo, Y., and Ouyang, S. (2019). Triaxial Compression Behaviour of Gangue Solid Wastes under Effects of Particle Size and Confining Pressure. *Sci. Total Environ.* 693, 133607. doi:10.1016/j.scitotenv.2019.133607

Huynh, L., Beattie, D. A., Fornasiero, D., and Ralston, J. (2006). Effect of Polyphosphate and Naphthalene Sulfonate Formaldehyde Condensate on the Rheological Properties of Dewatered Tailings and Cemented Paste Backfill. *Minerals Eng.* 19, 28–36. doi:10.1016/j.mineng.2005.05.001

Jiang, H., Fall, M., Yilmaz, E., Li, Y., and Yang, L. (2020). Effect of mineral Admixtures on Flow Properties of Fresh Cemented Paste Backfill: Assessment of Time Dependency and Thixotropy. *Powder Technol.* 372, 258–266. doi:10.1016/j.powtec.2020.06.009

Koohestani, B., Mokhtari, P., Yilmaz, E., Mahdipour, F., and Darban, A. K. (2021). Geopolymerization Mechanism of Binder-free Mine Tailings by Sodium Silicate. *Constr. Build. Mater.* 268, 121217. doi:10.1016/j.conbuildmat.2020.121217

Kou, Y., Jiang, H., Ren, L., Yilmaz, E., and Li, Y. (2020). Rheological Properties of Cemented Paste Backfill with Alkali-Activated Slag. *Minerals* 10 (3), 288. doi:10.3390/min10030288

Li, D. X. (2020). *Agricultural Waste Changes from "waste" to "treasure" to Promote green and Sustainable Development of Agriculture* Vegetables 7, 1–9.

Liao, Q., Li, B., and Wu, J. Y. (2018). Experimental Study on Preparation Technology of Straw Fiber Concrete. *Sichuan Build. Sci.* 44, 99–104. doi:10.19794/j.cnki.1008-1933.2018.02.019

Liu, G., Li, L., Yang, X., and Guo, L. (2016). Stability Analyses of Vertically Exposed Cemented Backfill: A Revisit to Mitchell's Physical Model Tests. *Int. J. Mining Sci. Technol.* 26, 1135–1144. doi:10.1016/j.ijmst.2016.09.024

Ma, G. W., Li, Z. J., Yi, X. W., and Guo, L. J. (2016). Macro-meso experiment of Fiber-Reinforced Cement Paste Filling Material. *J. Beijing Univ. Technol.* 42, 407–412. doi:10.11936/bjutxb2015040024

Mangane, M. B. C., Argane, R., Trauchessec, R., Lecomte, A., and Benzaazoua, M. (2018). Influence of Superplasticizers on Mechanical Properties and Workability of Cemented Paste Backfill. *Minerals Eng.* 116, 3–14. doi:10.1016/j.mineng.2017.11.006

Ming, X. L., Chen, H. T., and Wei, Z. P. (2019). Optimization of Technical Parameters for Making Light-Basis-Weight and Environment-Friendly rice Straw Fiber Film. *Trans. Chin. Soc. Agric. Eng.*, 259–266. doi:10.11975/j.issn.1002-6819.2019.19.032

Ouattara, D., Belem, T., Mbonimpa, M., and Yahia, A. (2018). Effect of Superplasticizers on the Consistency and Unconfined Compressive Strength of Cemented Paste Backfills. *Constr. Build. Mater.* 181, 59–72. doi:10.1016/j.conbuildmat.2018.05.288

Petrella, A., Spasiano, D., Liuzzi, S., Ayr, U., Cosma, P., Rizzi, V., et al. (2018). Use of Cellulose Fibers from Wheat Straw for Sustainable Cement Mortars. *J. Sustainable Cem.-Based Mater.* 3, 1–8. doi:10.1080/21650373.2018.1534148

Qi, C., and Fourie, A. (2019). Cemented Paste Backfill for mineral Tailings Management: Review and Future Perspectives. *Minerals Eng.* 144, 106025. doi:10.1016/j.mineng.2019.106025

Rahim, M., Douzane, O., Tran Le, A. D., Promis, G., and Langlet, T. (2016). Characterization and Comparison of Hygric Properties of Rape Straw concrete and Hemp concrete. *Constr. Build. Mater.* 102, 679–687. doi:10.1016/j.conbuildmat.2015.11.021

Ramli, M., Kwan, W. H., and Abas, N. F. (2013). Strength and Durability of Coconut-Fiber-Reinforced concrete in Aggressive Environments. *Constr. Build. Mater.* 38, 554–566. doi:10.1016/j.conbuildmat.2012.09.002

Sathiparan, N., and De Zoysa, H. T. S. M. (2018). The Effects of Using Agricultural Waste as Partial Substitute for Sand in Cement Blocks. *J. Build. Eng.* 19, 216–227. doi:10.1016/j.jobe.2018.04.023

Song, D. L., Hou, S. P., and Wang, X. B. (2018). The Amount of Straw Nutrient Resources in China and the Potential of Replacing Chemical Fertilizers. *J. Plant Nutr. Fert.* 24, 1–21. doi:10.11674/zwyf.17348

Sun, Z. F., and Jiang, E. C. (2007). Study on Mechanical Properties of rice Straw. *J. Northeast Agric. Univ.* 38 (5), 660–664. doi:10.19720/j.cnki.issn.1005-9369.2007.05.020

Wang, H.-Y., and Chen, K.-W. (2016). A Study of the Engineering Properties of CLSM with a New Type of Slag. *Constr. Build. Mater.* 102, 422–427. doi:10.1016/j.conbuildmat.2015.10.198

Wang, Y., Fall, M., and Wu, A. X. (2016). Initial Temperature-Dependence of Strength Development and Self-Desiccation in Cemented Paste Backfill that Contains Sodium Silicate. *Cem. Concr. Compos.* 67, 101–110. doi:10.1016/j.cemconcomp.2016.01.005

Wang, X. Y., Hu, C. G., and Feng, X. X. (2017). Strength of Modified Wheat Straw/Cement Composites. *J. Mater. Sci. Eng.* 35, 140–143. doi:10.14136/j.cnki.issn1673-2812.2017.01.028

Wang, S., Song, X., Chen, Q., Wang, X., Wei, M., Ke, Y., et al. (2020). Mechanical Properties of Cemented Tailings Backfill Containing Alkalized rice Straw of Various Lengths. *J. Environ. Manage.* 276, 111124. doi:10.1016/j.jenvman.2020.111124

Xie, X., Zhou, Z., Jiang, M., Xu, X., Wang, Z., and Hui, D. (2015). Cellulosic Fibers from rice Straw and Bamboo Used as Reinforcement of Cement-Based Composites for Remarkably Improving Mechanical Properties. *Compos. B: Eng.* 78, 153–161. doi:10.1016/j.compositesb.2015.03.086

Xie, X., Gou, G., Wei, X., Zhou, Z., Jiang, M., Xu, X., et al. (2016). Influence of Pretreatment of rice Straw on Hydration of Straw Fiber Filled Cement Based Composites. *Constr. Build. Mater.* 113, 449–455. doi:10.1016/j.conbuildmat.2016.03.088

Xu, W., Cao, Y., and Liu, B. (2019a). Strength Efficiency Evaluation of Cemented Tailings Backfill with Different Stratified Structures. *Eng. Struct.* 180, 18–28. doi:10.1016/j.engstruct.2018.11.030

Xu, W., Li, Q., and Zhang, Y. (2019b). Influence of Temperature on Compressive Strength, Microstructure Properties and Failure Pattern of Fiber-Reinforced Cemented Tailings Backfill. *Constr. Build. Mater.* 222, 776–785. doi:10.1016/j.conbuildmat.2019.06.203

Xue, G., Yilmaz, E., Song, W., and Yilmaz, E. (2019a). Influence of Fiber Reinforcement on Mechanical Behavior and Microstructural Properties of Cemented Tailings Backfill. *Constr. Build. Mater.* 213, 275–285. doi:10.1016/j.conbuildmat.2019.04.080

Xue, G., Yilmaz, E., Song, W., and Cao, S. (2019b). Mechanical, Flexural and Microstructural Properties of Cement-Tailings Matrix Composites: Effects of Fiber Type and Dosage. *Compos. Part B: Eng.* 172, 131–142. doi:10.1016/j.compositesb.2019.05.039

Xue, G., Yilmaz, E., Song, W., and Cao, S. (2020). Fiber Length Effect on Strength Properties of Polypropylene Fiber Reinforced Cemented Tailings Backfill Specimens with Different Sizes. *Constr. Build. Mater.* 241, 118113. doi:10.1016/j.conbuildmat.2020.118113

Yang, L., Qiu, J., Jiang, H., Hu, S., Li, H., and Li, S. (2017). Use of Cemented Super-fine Unclassified Tailings Backfill for Control of Subsidence. *Minerals* 7, 216. doi:10.3390/min7110216

Yang, L., Yilmaz, E., Li, J., Liu, H., and Jiang, H. (2018). Effect of Superplasticizer Type and Dosage on Fluidity and Strength Behavior of Cemented Tailings Backfill with Different Solid Contents. *Constr. Build. Mater.* 187, 290–298. doi:10.1016/j.conbuildmat.2018.07.155

Yang, L., Xu, W., Yilmaz, E., Wang, Q., and Qiu, J. (2020). A Combined Experimental and Numerical Study on the Triaxial and Dynamic Compression Behavior of Cemented Tailings Backfill. *Eng. Struct.* 219, 110957. doi:10.1016/j.engstruct.2020.110957

Yi, X. W., Ma, G. W., and Fourie, A. (2015). Compressive Behaviour of Fibre-Reinforced Cemented Paste Backfill. *Geotextiles Geomembr.* 43, 207–215. doi:10.1016/j.geotexmem.2015.03.003

Yilmaz, E., Belem, T., and Benzaazoua, M. (2015). Specimen Size Effect on Strength Behavior of Cemented Paste Backfills Subjected to Different Placement Conditions. *Eng. Geol.* 185, 52–62. doi:10.1016/j.enggeo.2014.11.015

Zeng, W., Huang, Z., Wu, Y., Li, S., Zhang, R., and Zhao, K. (2020). Experimental Investigation on Mining-Induced Strain and Failure Characteristics of Rock Masses of Mine Floor. *Geomatics, Nat. Hazards Risk* 11 (01), 491–509. doi:10.1080/19475705.2020.1734102

Zhang, X. Y., Lv, C., Zhang, D. M., Wang, L., and Li, Y. (2020). Performance of Increasing Toughness of Straw Fiber in Lightweight Aggregate concrete and its Prediction Model of Splitting Tensile Strength. *Mater. Rep.* 34 (02), 34–38.

Zhao, G. Y., Wu, H., Chen, Y., Xu, Z., Li, Z., and Wang, E. J. (2017). Experimental Study on Loadbearing Mechanism and Compaction Characteristics of Mine Filling Materials. *J. China Univ. Min. Technol.* 46, 1251–1258. doi:10.13247/j.cnki.jcumt.000759

Zheng, J., Zhu, Y., and Zhao, Z. (2016). Utilization of limestone Powder and Water-Reducing Admixture in Cemented Paste Backfill of Coarse Copper Mine Tailings. *Constr. Build. Mater.* 124, 31–36. doi:10.1016/j.conbuildmat.2016.07.055

Zheng, Y., Chen, C. X., Liu, T. T., and Ren, Z. H. (2021). A New Method of Assessing the Stability of Anti-dip Bedding Rock Slopes Subjected to Earthquake. *Bull. Eng. Geol. Environ.* 80 (4), 1–18. doi:10.1007/s10064-021-02188-4

Conflict of Interest: The authors declare that the research was conducted in the absence of any commercial or financial relationships that could be construed as a potential conflict of interest.

Publisher's Note: All claims expressed in this article are solely those of the authors and do not necessarily represent those of their affiliated organizations, or those of the publisher, the editors and the reviewers. Any product that may be evaluated in this article, or claim that may be made by its manufacturer, is not guaranteed or endorsed by the publisher.